PCCP

ROYAL SOCIETY OF CHEMISTRY

PAPER

View Article Online
View Journal | View Issue

Cite this: *Phys. Chem. Chem. Phys.*, 2024, **26**, 22931

IR spectrum of $SiH_3OH_2^+SiH_4$: cationic OH···HSi dihydrogen bond *versus* charge-inverted SiH···Si hydrogen bond†

Martin Andreas Robert George and Otto Dopfer *

Received 17th June 2024,
Accepted 11th August 2024

DOI: 10.1039/d4cp02428a

rsc.li/pccp

The low electronegativity of Si gives rise to a variety of nonconventional intermolecular interactions in clusters of silanes and their derivatives, which have not been well characterized yet. Herein, we characterize the structures of various isomers of bare and Ar-tagged $SiH_3OH_2^+SiH_4$ dimers composed of protonated silanol and silane by infrared photodissociation (IRPD) of mass-selected ions and dispersion-corrected density functional calculations (B3LYP-D3/aug-cc-pVTZ). The analysis of the IRPD spectra recorded in the OH stretch range reveals the competition between two types of nonconventional hydrogen bonds (H-bonds). The first one represents a OH···HSi ionic dihydrogen bond (DHB), in which SiH_4 interacts with the H_2O moiety of $SiH_3OH_2^+$. The second one represents a charge-inverted SiH···Si ionic H-bond (CIHB), in which the SiH_4 ligand interacts with the SiH_3 moiety of $SiH_3OH_2^+$. The latter may also be considered as a weak three-centre two-electron (3c–2e) bond. Although both types of H-bonds are computed to have comparable interaction strengths for $SiH_3OH_2^+SiH_4$ ($D_0 \approx 35$–40 kJ mol^{-1}), DHB isomers dominate the population in the supersonic plasma expansion, while the abundance of CIHB isomers is roughly one order of magnitude lower, probably as a result of entropic factors.

1. Introduction

Silanes (Si_xH_y), silanols ($Si_xH_yO_z$), and their derivatives are important molecules in inorganic chemistry, polymer and materials science, astrochemistry, plasma chemistry, and theoretical chemistry.[1–9] Laboratory spectra of silanes and their ions are essential to analyze and control the complex chemistry of silane plasmas used in semiconductor industry.[3,10–13] In addition, based on the detection of SiH_4 in the interstellar environment,[14] laboratory spectra of neutral and cationic $Si_xH_y^{(+)}$ and $Si_xH_yO_z^{(+)}$ molecules are needed for comparison with astronomical spectra.

Although Si is a group IV element like C, the chemical bonds in C_xH_y and Si_xH_y (and their ions) are quite different.[15] Part of these differences results from the lower electronegativity of Si (EN_{Si} = 1.90) compared to those of H and C (EN_H = 2.20, EN_C = 2.55). In general, Si–Si and Si–H bonds are longer than corresponding C–H and C–C bonds and exhibit more often nonclassical Si–H–Si bridges.[16–20] Such Si–H–Si bridges are three-center two-electron (3c–2e) bonds,[21,22] in which two electrons in a bonding orbital form two stable bonds in a more or less linear Si–H–Si bridge. These bridges can also be considered as strong charge-inverted hydrogen bonds (CIHBs) with polarity $Si^{\delta+}$–$H^{\delta-}$–$Si^{\delta+}$,[23–25] because EN_H is higher than EN_{Si}. We have previously characterized such ionic CIHBs in a variety of $Si_xH_y^+$ cations in the gas phase using infrared photodissociation spectroscopy (IRPD).[26–29] In addition, we recently presented the first spectroscopic and structural characterization of the highly elusive protonated silanol molecule ($SiH_3OH_2^+$) based on the IRPD spectrum of its Ar-tagged cluster.[30] While monosilanol (SiH$_3$OH) is rather unstable with respect to intermolecular condensation reactions and has hardly been characterized structurally and spectroscopically,[2] with the notable exception of a single IR band (ν_{SiO} = 859 cm^{-1}),[31] we could analyze the chemical bonding in $SiH_3OH_2^+$ and assign it to a dative bond of H_2O to the SiH_3^+ cation.

Herein, we report IRPD spectra of $SiH_3OH_2^+SiH_4$ and its Ar-tagged $SiH_3OH_2^+SiH_4$–Ar cluster to study the competition between two interesting and nonconventional types of intermolecular bonds between $SiH_3OH_2^+$ and SiH_4. The first one is the formation of a CIHB bond between SiH_4 and the SiH_3^+ moiety of $SiH_3OH_2^+$, which is typical for polysilane ions such as $Si_2H_7^+$ or longer $SiH_3^+(SiH_4)_n$ hydride wires,[26,29] but is affected in $SiH_3OH_2^+SiH_4$ by the dative bond of H_2O to SiH_3^+. The second binding motif is the formation of a cationic dihydrogen bond (DHB) of the type $Si^{\delta+}H^{\delta-}\cdots H^{\delta+}O^{\delta-}$ between the H_2O moiety of $SiH_3OH_2^+$ and the SiH_4 ligand, which represents a

Institut für Optik und Atomare Physik, Technische Universität Berlin, Berlin 10623, Germany. E-mail: dopfer@physik.tu-berlin.de

† Electronic supplementary information (ESI) available. See DOI: https://doi.org/10.1039/d4cp02428a

subclass of H-bond interactions.[32–46] The DHB is a H-bond interaction between two oppositely charged H atoms, which can only occur when one of the two H atoms is bonded to a more electropositive atom (*e.g.*, Si, B, transition metal) while the other H atom is bonded to a more electronegative atom (*e.g.*, O in our case). DHBs in systems with transition metals and B in their crystalline forms have been studied extensively.[32,34,35,47–56] In the gas phase, DHBs of the type BH···HO and BH···HN were investigated by IR spectroscopy and quantum chemical calculations.[42,57–63] The first spectroscopic evidence for a DHB of the type SiH···HO was reported by Ishikawa and co-workers in the phenol-diethylmethylsilane (PhDEMS) dimer.[64] Subsequently, SiH···HO bonds were found in phenol-triethylsilane (PhTES) and phenol-ethyldimethylsilane (PhEDMS), as well as in the related cationic Ph^+DEMS and Ph^+TES dimers.[65,66] The SiH···HO DHB is considered to be an intermediate motif in chemical reactions such as $H_2O + SiH_4 \rightarrow SiH_3OH + H_2$.[67,68] While neutral DHBs with Ph are weak and comparable to dispersion interactions, cationic DHBs are much stronger due to the much higher acidity of Ph^+ arising from its excess positive charge.[66] To gain a better understanding of the nature of the SiH···HO ionic DHBs, it is necessary to collect further spectroscopic information. To this end, we study in this work a significantly smaller system containing an ionic DHB, $SiH_3OH_2^+SiH_4$, to reveal the intrinsic nature of the SiH···HO DHB, which is the dominant intermolecular interaction in this cluster, without any interference from aromatic or aliphatic hydrocarbon structures.

2. Experimental and computational techniques

IRPD spectra of bare and Ar-tagged $SiH_3OH_2^+SiH_4$ ions in the OH stretch range (2700–3800 cm^{-1}) are obtained in a tandem quadrupole mass spectrometer coupled to an electron ionization (EI) source described elsewhere.[69–72] $SiH_3OH_2^+SiH_4$ and $SiH_3OH_2^+SiH_4$–Ar clusters are generated in a pulsed supersonic plasma expansion of a SiH_4/He/Ar gas mixture (ratio 1 : 20 : 200, 5 bar stagnation pressure) seeded with H_2O vapor. The gas mixture is ionized by EI (and/or chemical ionization), resulting in the formation of a variety of hydrated silicon hydride cluster cations and their Ar complexes. The rather stable silyl cation (SiH_3^+) is the major primary EI product of SiH_4. In a next step, protonated silanole is produced *via* barrierless addition of H_2O to SiH_3^+ forming a rather stable chemical Si–O bond in $SiH_3OH_2^+$.[30] In subsequent three-body aggregation reactions occurring in the high-pressure region of the expansion, weakly-bound clusters of $SiH_3OH_2^+$ with SiH_4 and Ar are generated and cooled down to lower temperatures. A typical mass spectrum of the EI source reveals strong Ar_n^+ cluster signals, accompanied by weaker peaks arising from OH_{1-2}^+, $Si_xH_y^+$, $Si_xH_yO^+$, and their Ar clusters (Fig. S1, ESI†). After extraction through a skimmer, bare or Ar-tagged $SiH_3OH_2^+SiH_4$ ions (*m/z* 81 or 121) are selected by the first quadrupole mass filter and irradiated in an adjacent octupole with tunable IR laser radiation generated by an optical parametric IR oscillator pumped by a nanosecond Q-switched Nd:YAG laser. The IR radiation is characterized by a pulse energy of ~1–5 mJ in the employed spectral range, a repetition rate of 10 Hz, and a bandwidth of 1 cm^{-1}. Calibration of the IR laser frequency (ν_{IR}) is accomplished by a wavemeter. Resonant vibrational excitation of $SiH_3OH_2^+SiH_4$(–Ar) induces the rupture of the weakest intermolecular bond (*i.e.*, loss of Ar or SiH_4). The resulting $SiH_3OH_2^+(SiH_4)$ fragment ions are selected by the second quadrupole mass filter and monitored as a function of ν_{IR} to derive the IRPD spectra of $SiH_3OH_2^+SiH_4$(–Ar). To separate the fragment ions produced by metastable decay from those generated by laser-induced dissociation, the ion source is triggered at twice the laser frequency, and signals from alternating triggers are subtracted. The widths of the observed transitions result from unresolved rotational substructure and overlapping sequence hot bands of intramolecular fundamentals with low-frequency intermolecular modes and possibly lifetime broadening. Because the population of rotational levels of the parent ions generated in this supersonic plasma expansion cannot be described by a single rotational temperature due to the lack of thermal equilibrium (levels with larger rotational quantum numbers are populated according to a higher temperature), we cannot readily simulate a rotational band profile. In addition, as the time-of-flight in the octupole is of the order of one millisecond, we do not observe a kinetic shift and all photoexcited ions with a final energy larger than the dissociation energy contribute to the measured IRPD yield. The IRPD yield is normalized for laser intensity variations measured with a pyroelectric detector. Because the mass spectrum of the ion source is rather complex, collision-induced dissociation (CID) experiments are employed to confirm the composition of the investigated $SiH_3OH_2^+SiH_4$(–Ar) parent ions. To this end, the octupole is filled with 10^{-5} mbar of N_2, allowing for collisions with mass-selected ions at a kinetic energy of 10 eV in the laboratory frame. Clearly, the CID spectrum of mass-selected $SiH_3OH_2^+$-SiH_4–Ar (*m/z* 121) demonstrates the almost exclusive loss of Ar followed by loss of SiH_4 resulting in $SiH_3OH_2^+$ (*m/z* 49), confirming its composition (Fig. S2, ESI†). A very minor channel follows the other sequence (primary loss of SiH_4 followed by loss of Ar).

Quantum chemical calculations are performed at the dispersion-corrected B3LYP-D3/aug-cc-pVTZ level of theory for SiH_4, $SiH_3OH_2^+$, and various isomers of $SiH_3OH_2^+SiH_4$(–Ar) to determine their energetic, structural, vibrational, and electronic properties.[73] This computational level reliably reproduces the properties of $SiH_3OH_2^+$ and its $SiH_3OH_2^+$–$Ar_{n\leq 5}$ complexes and the 3c–2e bonds in $Si_xH_{4x-1}^+$ hydride wires.[29,30] Relative energies and equilibrium binding energies (E_e, D_e) are corrected for harmonic zero-point vibrational energies to derive E_0 and D_0 values. Gibbs free energies (G_0) are evaluated at 298.15 K. Harmonic frequencies are scaled by factors of 0.9631 (0.9805) for frequencies above (below) 2000 cm^{-1} to optimize the agreement between calculated and measured frequencies of H_2O.[30] Natural bond orbital (NBO) analysis is employed to evaluate the charge distribution and charge transfer, as well as the second-order perturbation energies ($E^{(2)}$) of donor–acceptor orbital interactions involved in the H-bonds. Calculated

vibrational frequencies are compared with experimental values in Tables S1–S3 (ESI†), and calculated energies are listed in Tables S4–S9 (ESI†).

3. Results and discussion

3.1 Overview of IRPD spectra

IRPD spectra of $SiH_3OH_2^+SiH_4$ and $SiH_3OH_2^+SiH_4$–Ar recorded in the OH stretch range are compared in Fig. 1 to that of $SiH_3OH_2^+$–Ar reported previously.[30] The positions, widths, and suggested vibrational and isomer assignments are listed in Table 1. For a detailed discussion of the properties of $SiH_3OH_2^+$ and $SiH_3OH_2^+$–Ar, we refer to our previous work.[30] Because of the strong bonds in bare $SiH_3OH_2^+$, no IRPD spectrum can be obtained for this ion under the employed single-photon absorption conditions. Its symmetric and antisymmetric OH stretch fundamentals ($\nu_{OH}^{s/a}$) computed as 3550 and 3626 cm^{-1} are indicated by grey dashed lines in Fig. 1. The splitting of 76 cm^{-1} between ν_{OH}^{s} and ν_{OH}^{a} results from the coupling of the two equivalent local OH stretch oscillators. The $SiH_3OH_2^+$–Ar spectrum shows two OH stretch bands **C1** and **E** at 3400 and 3600 cm^{-1}, which can readily be attributed to the Ar-bonded

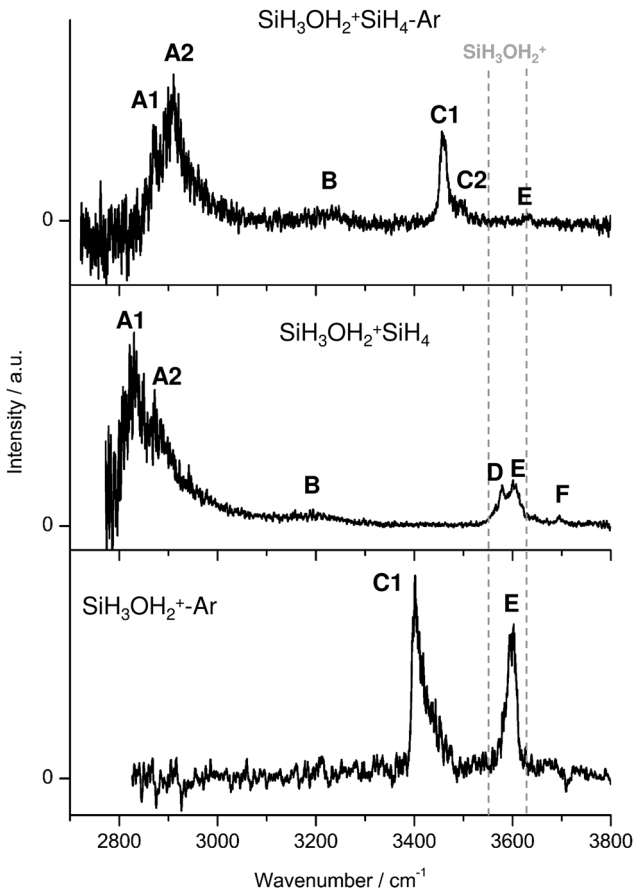

Fig. 1 IRPD spectra of $SiH_3OH_2^+SiH_4$ and $SiH_3OH_2^+SiH_4$–Ar in the 2700–3800 cm^{-1} range recorded in the SiH_4 and Ar loss channels, respectively, are compared to the IRPD spectrum of $SiH_3OH_2^+$–Ar.[30] The position, widths, and assignments of the transitions observed are listed in Table 1 and Tables S1–S3 (ESI†).

and free OH stretch modes ($\nu_{OH}^{b(Ar)}$ and ν_{OH}^{f}) of the global minimum structure, in which Ar forms an OH···Ar H-bond to one of the two OH groups of $SiH_3OH_2^+$. The assignment of these two bands is not only supported by their frequencies and shifts from those of bare $SiH_3OH_2^+$ but also by their band profiles. While the free OH stretch band has a symmetric profile, the Ar-bonded OH stretch band has a sharp P-branch head and a long blueshaded tail, which are typical for excitation of proton donor stretch modes.[70,74,75] Excitation of a proton-donor stretch fundamental causes the H-bond to become stronger, leading to smaller rotational constants in the vibrational excited state, giving rise to a P-branch head. In addition, the stronger H-bond in the intramolecular excited state causes the intermolecular stretch and bend frequencies to be larger than in the ground vibrational state due to the larger radial force constant and larger angular anisotropy in the intermolecular potential. Hence, sequence hot bands of the proton-donor stretch fundamental with intermolecular modes appear to the blue of the fundamental transition. These effects to not operate for excitation of the free OH stretch mode and, as a result, such bands exhibit a symmetric band shape. Complexation with Ar removes the coupling between the two OH stretch oscillators. As a result, the ν_{OH}^{f} band of $SiH_3OH_2^+$–Ar occurs roughly at the average frequency of ν_{OH}^{s} and ν_{OH}^{a} of bare $SiH_3OH_2^+$ predicted as 3588 cm^{-1}, while the $\nu_{OH}^{b(Ar)}$ band of $SiH_3OH_2^+$–Ar is redshifted by almost 200 cm^{-1} from this value due to the formation of the OH···Ar H-bond. The $SiH_3OH_2^+SiH_4$ spectrum is dominated by strongly redshifted $\nu_{OH}^{b(SiH_4)}$ bands **A1** and **A2** (by around 750 cm^{-1}) near 2850 cm^{-1} indicative of the formation of a much stronger OH···SiH_4 H-bond. This observation is consistent with the larger polarizability of SiH_4 compared to Ar (computed as α = 32.20 *vs.* 11.15 a_0^3), because induction and dispersion interactions provide the major contribution to the intermolecular attraction. The intense **A1** band peaks at 2830 cm^{-1} with a width of 40 cm^{-1}, while the weak shoulder **A2** has its maximum at 2872 cm^{-1}. In addition, three bands **D–F** appear in the free OH stretch range above 3500 cm^{-1}, suggesting the presence of at least two isomers. The strongest band **E** at 3602 cm^{-1} has almost the same frequency as band **E** in the $SiH_3OH_2^+$ spectrum, indicating an assignment to the free OH stretch (ν_{OH}^{f}) of a cluster with a strong OH···SiH_4 H-bond. On the other hand, bands **D** and **F** at 3578 and 3695 cm^{-1} occur not far from the free OH stretch bands ν_{OH}^{s} and ν_{OH}^{a} of bare $SiH_3OH_2^+$ predicted at 3550 and 3626 cm^{-1} suggesting the presence of an isomer, in which the SiH_4 ligand is not attached to the OH_2 side of $SiH_3OH_2^+$ but to the SiH_3 side. Ar-tagging of $SiH_3OH_2^+SiH_4$ causes modest blue shifts of the **A1**/**A2** bands (to 2869/2910 cm^{-1}) and produces an intense band **C1** at 3456 cm^{-1} (with a width of 15 cm^{-1}) characteristic for a complex with one OH···SiH_4 and one OH···Ar H-bond. Such small blueshifts in proton donor stretch vibrations (like here for **A1**/**A2**) are characteristic for interior ion solvation, which is accompanied by small noncooperative effects on the H-bond strengths due to increased charge delocalization into a larger number of neutral ligands. The presence of the weaker bands **C2** and **E** in the OH stretch range

Table 1 Position and widths (in cm^{-1}) of the transitions observed in the IRPD spectra of $SiH_3OH_2^+SiH_4$ and $SiH_3OH_2^+SiH_4$–Ar compared to frequencies of $SiH_3OH_2^+$–Ar

	Isomer[a]	Mode	$SiH_3OH_2^+$–Ar[c]	$SiH_3OH_2^+SiH_4$	$SiH_3OH_2^+$ SiH_4–Ar
A1	DHB	$\nu_{OH}^{b(SiH_4)}$	—	2830 (40)	2869 (15)
A2	DHB	$\nu_{OH}^{b(SiH_4)}$	—	2872 (40)	2910 (40)
B	DHB/CIHB	$2\beta_{OH}^{b}$	—	~3190	~3230
C1	DHB	$\nu_{OH}^{b(Ar)}$	3400 (21)	—	3456 (15)
C2	CIHB	$\nu_{OH}^{b(Ar)}$	—	—	3495 (20)
D	CIHB	ν_{OH}^{s}	—	3578 (20)	—
E	DHB/CIHB	ν_{OH}^{f}	3600 (30)	3602 (30)	3629 (15)
F	CIHB	$\nu_{OH}^{a\,b}$	—	3695 (10)	—

[a] Intermolecular binding motifs of isomers **I–III** (DHB) and **IV** (CIHB) of $SiH_3OH_2^+SiH_4$ and $SiH_3OH_2^+SiH_4$–Ar are assigned to the observed transitions (and do not apply to $SiH_3OH_2^+$–Ar). [b] Tentative assignment. [c] Ref. 30.

at 3495 and 3629 cm^{-1} is again indicative of a less stable isomer in which one OH group of the $SiH_3OH_2^+$ core ion is not engaged in a H-bond (ν_{OH}^{f}) while the other one forms an OH···Ar H-bond ($\nu_{OH}^{b(Ar)}$). In such an isomer, the SiH_4 ligand does not bind to one of the OH groups of $SiH_3OH_2^+$ but to its SiH_3 moiety. The IRPD spectra of both bare and Ar-tagged $SiH_3OH_2^+$-SiH_4 reveal a weak band **B** at ~3190 and ~3230 cm^{-1}, respectively, which is not present in the $SiH_3OH_2^+$–Ar spectrum. They may arise either from the β_{OH} overtone of the H_2O moiety or a combination band of the SiH_4-bound OH stretch fundamentals with an intermolecular mode. The latter scenario may be supported by the blueshift in band **B** upon Ar-tagging (~20 cm^{-1}), which parallels the blue shifts of bands **A1**/**A2** (~40 cm^{-1}).

In summary, the initial analysis of the IRPD spectra of bare and Ar-tagged $SiH_3OH_2^+SiH_4$ reveals two routes of cluster growth. Along the predominant path, SiH_4 and Ar form intermolecular H-bonds to the two available acidic OH groups of $SiH_3OH_2^+$, while a minor route involves attachment of SiH_4 to the SiH_3 moiety, whereas Ar then forms a OH···Ar H-bond. To derive more details of this preliminary analysis based on the IRPD spectra alone, we resort to quantum chemical calculations.

3.2 Computational analysis and assignments

3.2.1 $SiH_3OH_2^+$, $SiH_3OH_2^+$–Ar, and SiH_4. The structural, vibrational, and electronic properties of $SiH_3OH_2^+$(–Ar) have been described in detail previously and only the salient results relevant for the present work are briefly summarized.[30] The global minimum of $SiH_3OH_2^+$ with C_s symmetry is generated by dative bonding of a H_2O lone pair to the vacant and electrophilic $3p_z$ orbital of SiH_3^+, leading to a strong chemical Si–O bond (1.851 Å, 219 kJ mol^{-1}). The barriers for internal SiH_3 rotation and inversion of the slightly pyramidal oxonium moiety are rather small (<0.3 kJ mol^{-1}). The free OH stretch fundamentals are predicted at ν_{OH}^{s} = 3550 and ν_{OH}^{a} = 3626 cm^{-1} with high IR intensity (232 and 319 km mol^{-1}). The large positive partial charges of q_H = 0.563 and q_{Si} = 1.186 *e* on the two acidic H atoms and Si, make these atoms attractive binding sites for both SiH_4 and Ar ligands. Ar preferentially forms a weak OH···Ar ionic H-bond in the $SiH_3OH_2^+$–Ar(H) isomer, characterized by a bond length of 2.176 Å, a modest binding energy of D_0 = 16.1 kJ mol^{-1}, a donor–acceptor energy of $E^{(2)}$ = 38.7 kJ mol^{-1}, and a charge transfer from $SiH_3OH_2^+$ to Ar of 35 m*e*. Consequently, the IRPD spectrum of $SiH_3OH_2^+$–Ar reproduced in Fig. 1 exhibits a redshifted Ar-bound OH stretch band **C1** at $\nu_{OH}^{b(Ar)}$ = 3400 cm^{-1} and a free OH stretch band **E** at ν_{OH}^{f} = 3600 cm^{-1}, in good agreement with the computational predictions (3369 and 3602 cm^{-1}, Table S1, ESI†). The less stable $SiH_3OH_2^+$Ar(Si) isomer with a much weaker Ar···Si bond (R = 3.165 Å, D_0 = 9.6 kJ mol^{-1}) is not observed in the measured IRPD spectrum.

The tetrahedral SiH_4 molecule has a computed Si–H bond length and vibrational frequencies (1.484 Å and ν_{1-4} = 2150, 966, 2151, 906 cm^{-1}), in good agreement with available experimental data (1.480 Å and 2187, 975, 2191, 914 cm^{-1}).[76,77] Significantly, because of the negative partial charges of its H atoms (q_H = −0.161 *e*), they are attracted by the positive charge centres of $SiH_3OH_2^+$ (OH and Si) to form ionic SiH···HO and SiH···Si H-bonds.

3.2.2 $SiH_3OH_2^+SiH_4$. On the basis of the $SiH_3OH_2^+$ structure, the four stable $SiH_3OH_2^+SiH_4$ isomers shown in Fig. 2 are obtained by adding SiH_4 to either an OH group (**I–III**) or Si (**IV**) and their relative energies and binding energies are listed in Table S4 (ESI†). Corresponding IR spectra are compared in Fig. 3 to the measured IRPD spectrum and the suggested vibrational and isomer assignments are listed in Table S2 (ESI†). NBO charge distributions are available in Fig. S3 (ESI†).

In the three most stable isomers (**I–III**), SiH_4 binds to one of the two equivalent OH groups of $SiH_3OH_2^+$ *via* a rather strong OH···HSi ionic DHB with very similar binding energies (D_0 = 38.9, 38.7, 38.5 kJ mol^{-1}, $\Delta D_0 \leq$ 0.4 kJ mol^{-1}). These conformers differ mainly in the orientation of the SiH_4 ligand. SiH_4 binds with one of its negative H atoms (q_H = −282, 286, −267 m*e*) to a positive H atom (q_H = 549, 548, 548 m*e*) of the OH group at intermolecular bond distances of R = 1.397, 1.389, and 1.418 Å in almost linear OH···H ionic DHBs (θ = 173.3°, 175.8°, 175.0°). The SiH···H bond angles deviate significantly more from linearity (θ = 131.3°, 134.2°, 125.1°), indicating a rather small angular anisotropy of the potential for the orientation of the SiH_3 group when optimizing dispersion and induction forces. The DHB involves substantial charge transfer from $SiH_3OH_2^+$ to SiH_4 (Δq = 81, 81, 80 m*e*), consistent with the large $E^{(2)}$ energies describing the strong interaction between the bonding σ_{SiH} orbital and the antibonding σ_{OH}^* orbital (99.4, 101.0, 96.1 kJ mol^{-1}). Upon formation of the strong OH···HSi

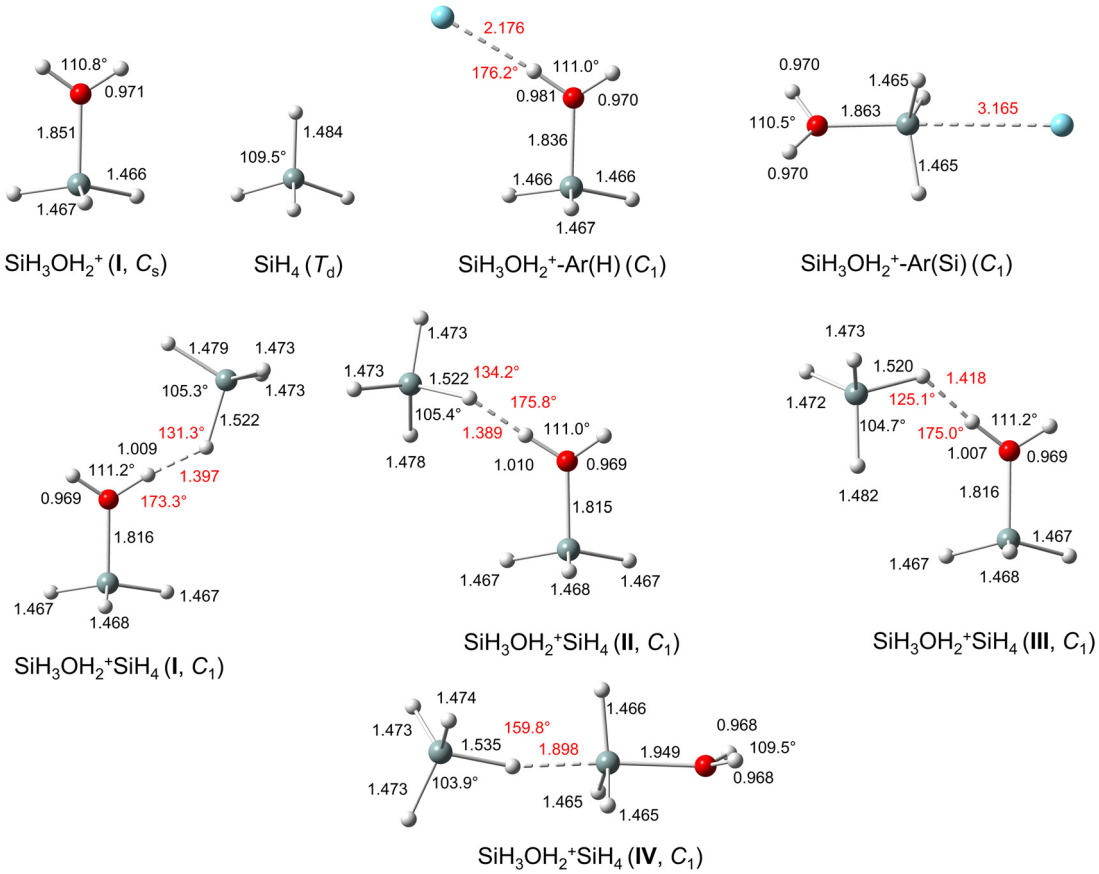

Fig. 2 Calculated equilibrium structures (in Å and degrees) of SiH_4, $SiH_3OH_2^+$, $SiH_3OH_2^+$–Ar(H), $SiH_3OH_2^+$–Ar(Si), and $SiH_3OH_2^+SiH_4$(**I–IV**) in their ground electronic state (B3LYP-D3/aug-cc-pVTZ).

DHBs, both proton donor bonds are strongly elongated (Δr_{SiH} = 38, 38, 36 mÅ, Δr_{OH} = 38, 39, 36 mÅ). As a result, the ν_{OH}^{b} modes are massively redshifted from ν_{OH}^{s} = 3550 cm^{-1} in bare $SiH_3OH_2^+$ down to $\nu_{OH}^{b(SiH_4)}$ = 2858, 2851, and 2885 cm^{-1} for **I–III**, respectively. These large redshifts of around 700 cm^{-1} are accompanied by a drastic increase in IR intensity by a factor of 10. In contrast, the free O–H bonds of all three isomers contract slightly (Δr_{OH} = −2 mÅ) causing corresponding minor blueshifts of the order of 20 cm^{-1} from the averaged free OH stretch frequency of $SiH_3OH_2^+$ (3588 cm^{-1}) to ν_{OH}^{f} = 3608, 3605, and 3611 cm^{-1}. These occur to the red of ν_{OH}^{a} of $SiH_3OH_2^+$ (3626 cm^{-1}), because SiH_4 complexation of one OH group removes the strong coupling between the two free and equivalent OH local modes in the monomer ($\Delta\nu_{OH}$ = 76 cm^{-1}). Furthermore, the DHB of $SiH_3OH_2^+$ to SiH_4 shortens the Si–O bond from 1.851 to 1.816 (**I**/**III**) and 1.815 Å (**II**), while the O–H–O bond angle increases slightly from 110.8° to 111.2°(**I**/**III**) and 111.0° (**II**).

In contrast to the DHB isomers **I–III**, SiH_4 is attached in **IV** to the Si atom of $SiH_3OH_2^+$ *via* an ionic Si–H–Si (SiH···Si) CIHB (R = 1.898 Å, D_0 = 36.2 kJ mol^{-1}). This CIHB is only slightly less stable than the DHB by ΔE_0 = 2.6 kJ mol^{-1} at the B3LYP-D3 level. Moreover, it is nonlinear (θ = 159.8°), as is typical for CIHBs,[24] and may be considered as a rather asymmetric 3c–2e Si–H–Si bond (R = 1.535 and 1.898 Å). The Si–H proton donor bond is elongated from 1.484 to 1.535 Å (Δr_{SiH} = 51 mÅ). The NBO analysis reveals a larger charge transfer from $SiH_3OH_2^+$ to SiH_4 (159 m*e*) and also a larger $E^{(2)}$ energy (167.9 kJ mol^{-1}) from the bonding σ_{SiH} orbital to the lone pair orbital of Si (LP_{Si}*) when compared to the DHB. In contrast to **I–III**, complexation with SiH_4 in **IV** leads to a strong elongation of the Si–O bond by 98 mÅ and a minor contraction of the O–H bonds by 3 mÅ. As a result, both $\nu_{OH}^{a/s}$ modes are blueshifted by 37 cm^{-1} to $\nu_{OH}^{s/a}$ = 3587/3662 cm^{-1}, while the coupling between both OH stretch oscillators remains similar (75 *vs.* 76 cm^{-1}).

Comparison of the IRPD spectrum of $SiH_3OH_2^+SiH_4$ with the linear IR spectra computed for the four isomers **I–IV** in Fig. 3 immediately confirms the presence of isomers with a DHB, as the IRPD spectrum is dominated by the intense and strongly redshifted $\nu_{OH}^{b(SiH_4)}$ bands **A1** and **A2** caused by SiH_4 binding to the OH_2 group. The strongest transition **A1** at 2830 cm^{-1} is assigned to the $\nu_{OH}^{b(SiH_4)}$ modes of **I** and **II** with deviations of 28 and 21 cm^{-1}, while peak **A2** at 2872 cm^{-1} may tentatively be attributed to the slightly less redshifted $\nu_{OH}^{b(SiH_4)}$ mode of **III** at 2885 cm^{-1}. Alternatively, this weak satellite band may also arise from sequence hot bands of $\nu_{OH}^{b(SiH_4)}$ with intermolecular modes, which are typical for the excitation of proton donor stretch modes.[70,74,75] The corresponding ν_{OH}^{f} modes of **I–III** can be assigned to band **E** at 3602 cm^{-1} with minor deviations of 6, 3, and 9 cm^{-1}. However, band **F** at 3695 cm^{-1} cannot be rationalized by any isomer with a DHB due to its high

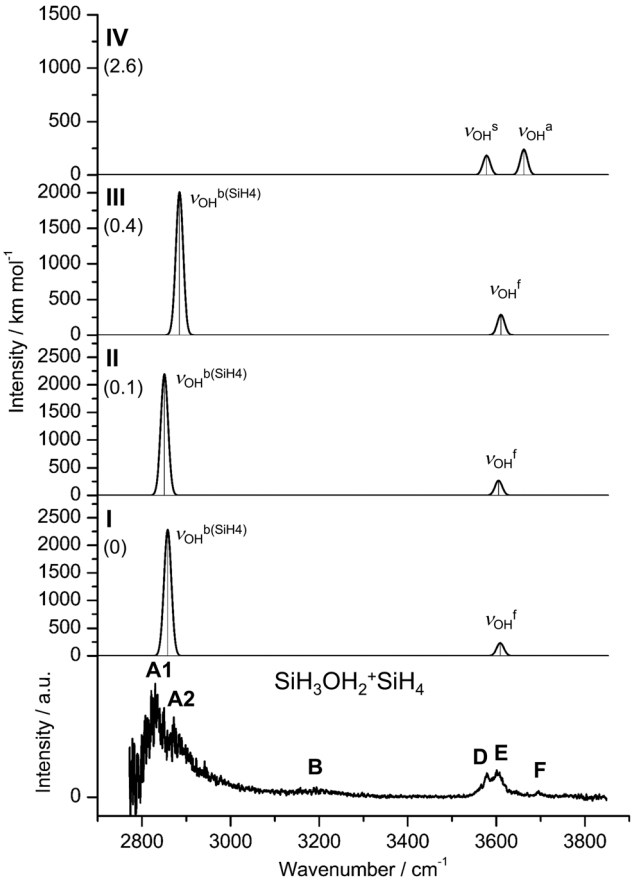

Fig. 3 IRPD spectrum of $SiH_3OH_2^+SiH_4$ compared to linear IR absorption spectra of isomers **I–IV** calculated at the B3LYP-D3/aug-cc-pVTZ level. The positions of the transition observed in the IRPD spectrum of $SiH_3OH_2^+SiH_4$ and their vibrational assignment are listed in Table S2 (ESI†). Differences in relative energy (E_0) are given in kJ mol^{-1} (in parentheses).

frequency. Instead, along with band **D** at 3578 cm^{-1}, these transitions can arise from the coupled free OH stretch modes $\nu_{OH}^{s/a}$ of **IV** predicted at 3587 and 3662 cm^{-1}, respectively. From the integrated intensities of the bands **A1**/**A2** and **D** (accounting for the shoulder of **E**) and the computed IR intensities, a population ratio of 10 : 1 can roughly be estimated for isomers with a DHB (**I–III**) and isomers with a CIHB (**IV**). The intensity ratios of bands **D** and **E** are consistent with this rough population ratio. While the predominant production of isomers **I–III** over **IV** is consistent with their slightly larger binding energies computed at the B3LYP-D3 level (D_0 = 39 *vs.* 36 kJ mol^{-1}), their rather large fractional abundance appears at first glance surprising in view of the similar computed stabilities. However, when considering the free entropy values, the ΔE_0 difference between **I** and **IV** of 2.6 kJ mol^{-1} increases to ΔG_0 = 4.1 kJ mol^{-1}. Finally, their appear to be several more low-energy (local) DHB minima than CIHB minima, which may further enhance the population of the former type of isomers for statistical reasons. In addition, the DHB minima are doubly degenerate because of the two equivalent OH groups of $SiH_3OH_2^+$, which may again favor the presence of DHB over CIHB isomers. To test whether the energy difference between both types of isomers changes with the computational level, single-point energy calculations are conducted at the CCSD(T)/aug-cc-pVTZ level, yielding actually a slightly larger binding energy (not corrected for zero-point energy) for **IV** than for **I** (D_e = 40.4 *vs.* 36.5 kJ mol^{-1}). Similarly, the binding energies obtained at the GBS-QB3 level are also slightly in favor of **IV** (D_0 = 34.4 *vs.* 33.0 kJ mol^{-1}), while again the free energy values slightly favor **I** over **IV** (by 1.9 kJ mol^{-1}). Hence, the considered computational levels predict rather similar binding energies for the DHB and CIHB isomers but entropy factors apparently favor the formation of DHB isomers, in agreement with the experimental observation. The weak transition **B** at 3194 cm^{-1} is probably an overtone or combination band and may be assigned for example to the first overtone of the β_{OH} bending mode predicted at 3212, 3222, 3216, and 3228 cm^{-1} of **I–IV** neglecting anharmonicity effects. Finally, the B3LYP-D3 binding energies of 35–40 kJ mol^{-1} ($\sim$2900–3350 cm^{-1}) are of the same order as the photon energies of the transitions observed in the investigated spectra range ($\sim$2800–3700 cm^{-1}), indicating that single-photon dissociation of the SiH_4 ligand is feasible for all isomers, even for those with no or only little rovibrational internal excitation.

3.2.3 $SiH_3OH_2^+SiH_4$–Ar. To confirm the vibrational and isomer assignments given for $SiH_3OH_2^+SiH_4$, IRPD spectra of colder Ar-tagged ions are considered. As most of the Ar-tagged isomers of **I–IV** differ only slightly in their IRPD spectra, we focus in Fig. 4 on the most stable ones derived from the two structural classes **I** (DHB) and **IV** (CIHB). The IR spectra of **I**-Ar(**I**,**II**) are representative of isomers with a DHB, while **IV**-Ar(**I**) is the most stable structure representing isomers with a CIHB. A description of other $SiH_3OH_2^+SiH_4$–Ar isomers may be found in ESI.† Specifically, the linear IR spectra of (**I–IV**)-Ar(**I–IV**) are compared in Fig. S4–S7 (ESI†) to the spectra computed for the corresponding untagged $SiH_3OH_2^+SiH_4$ isomers and the IRPD spectrum measured for $SiH_3OH_2^+SiH_4$–Ar. The vibrational and isomer assignments are listed in Table S3, and all relevant energies are provided in Tables S5–S9 (ESI†).

In the most stable **I**-Ar(**I**) isomer, Ar binds to the remaining free OH group of $SiH_3OH_2^+SiH_4$(**I**) *via* an OH$\cdots$Ar H-bond (R = 2.228 Å, D_0 = 14.0 kJ mol^{-1}). Due to noncooperative three-body effects of interior ion solvation arising from enhanced charge delocalization, this H-bond is somewhat weaker than that in H-bonded $SiH_3OH_2^+$–Ar with only one ligand (R = 2.176 Å, D_0 = 16.1 kJ mol^{-1}), with correspondingly smaller impact on the intramolecular properties of $SiH_3OH_2^+$. The H-bond in **I**-Ar(**I**) slightly elongates the O–H proton donor bond by 7 mÅ and contracts the adjacent O–H bond by 5 mÅ, resulting in a $\nu_{OH}^{b(Ar)}$ redshift of 160 cm^{-1} to 3448 cm^{-1} and a $\nu_{OH}^{b(SiH_4)}$ blueshift of 76 cm^{-1} to 2934 cm^{-1}. As a consequence of the stronger O–H bond interacting with SiH_4, Ar attachment leads to a destabilization of the OH$\cdots$HSi DHB, which elongates by 16 mÅ. In the corresponding **II**/**III**-Ar(**I**) isomers (E_0^{tot} = 0.3 and 0.9 kJ mol^{-1}), Ar is also H-bonded to the free OH group at similar distances (R = 2.223/2.226 Å) with similar binding energies (D_0 = 13.8/13.5 kJ mol^{-1}) and comparable shifts of the $\nu_{OH}^{b(Ar)}$ (3442 cm^{-1}) and $\nu_{OH}^{b(SiH_4)}$ modes (2925, 2958 cm^{-1}) (Fig. S5 and S6, ESI†).

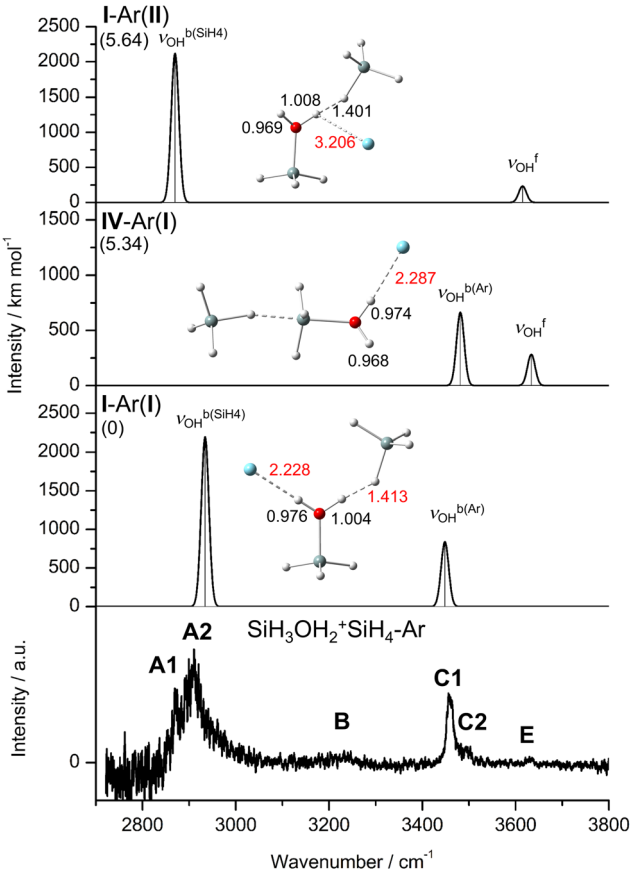

Fig. 4 IRPD spectrum of $SiH_3OH_2^+SiH_4$–Ar compared to linear IR absorption spectra of **I**-Ar(**I**), **IV**-Ar(**I**) and **I**-Ar(**II**) together with their equilibrium structures (in Å) calculated at the B3LYP-D3/aug-cc-pVTZ level. The positions of the transition observed in the IRPD spectrum of $SiH_3OH_2^+SiH_4$–Ar and their vibrational assignment are listed in Table S3 (ESI†). Differences in relative energy (E_0) are given in kJ mol^{-1}.

In the less stable **I**-Ar(**II**) isomer (E_0 = 5.6 kJ mol^{-1}), Ar is bound perpendicularly to the OH proton of **I** (θ_{OHAr} = 96.5°, R = 3.206 Å, D_0 = 8.3 kJ mol^{-1}) engaged in the DHB. As a result, this O–H bond contracts slightly (by 1 mÅ) leading to a small blueshift (by 12 cm^{-1}) of the corresponding $\nu_{OH}^{b(SiH_4)}$ mode to 2870 cm^{-1} when compared to **I**. On the other hand, the DHB in **I**-Ar(**II**) is stronger than in **I**-Ar(**II**) (R = 1.401 *vs.* 1.413 cm^{-1}), causing a larger redshift in $\nu_{OH}^{b(SiH_4)}$ (2870 *vs.* 2934 cm^{-1}). In the corresponding **II**-Ar(**II**) isomer (E_0^{tot} = 5.9 kJ mol^{-1}), Ar has a similar binding motif, resulting in a comparable blueshift of $\nu_{OH}^{b(SiH_4)}$ (2869 cm^{-1}) so that it cannot be distinguished (Fig. S5, ESI†).

In the most stable **IV**-Ar(**I**) isomer featuring a Si–H–Si bond (E_0^{tot} = 5.3 kJ mol^{-1}), Ar is slightly less H-bonded to one of the free OH groups (R = 2.287 Å, D_0 = 11.3 kJ mol^{-1}) than in **I**-Ar(**I**). This OH···Ar H-bond elongates the O–H proton donor bond by 6 mÅ and contracts the adjacent free O–H bond by 1 mÅ. As a result, $\nu_{OH}^{b(Ar)}$ of **IV**-Ar(**I**) is redshifted by 105 cm^{-1} to 3482 cm^{-1} while ν_{OH}^{f} is less redshifted by 29 cm^{-1} to 3633 cm^{-1}. In **IV**-Ar(**II**) (E_0^{tot} = 5.6 kJ mol^{-1}), Ar is bound to the other free OH group with a binding energy of D_0 = 11.0 kJ mol^{-1}, resulting in very similar shifts to $\nu_{OH}^{b(Ar)}$ = 3482 cm^{-1} and ν_{OH}^{f} = 3634 cm^{-1} as for **IV**-Ar(**I**).

In the less stable (**I**–**III**)-Ar(**III**) isomers (E_0^{tot} = 6.3, 6.4, 6.5 kJ mol^{-1}), Ar is Si-bonded to the SiH_3 group (D_0 = 7.7, 7.8, 7.9 kJ mol^{-1}), which affects the O–H bond of the DHB of **I**–**III** leading to small blueshifts of $\nu_{OH}^{b(SiH_4)}$ by 43, 45, and 45 cm^{-1} to 2901, 2896, and 2930 cm^{-1}, respectively (Fig. S4–S6, ESI†). In **IV**-Ar(**III**) (E_0^{tot} = 10.7 kJ mol^{-1}), Ar is bound almost perpendicularly to the H atom of the Si–H–Si bridge (R = 3.396 Å, D_0 = 5.9 kJ mol^{-1}, Fig. S7, ESI†). This affects the Si–H–Si bridge by shortening the Si–H and SiH···Si bonds by 2 and 3 mÅ but has almost no effect on the O–H bonds and their vibrational modes. The same is true for **IV**-Ar(**IV**) (E_0^{tot} = 12.6 kJ mol^{-1}), in which Ar binds to the Si atom of the SiH_4 ligand (R = 3.563 Å, D_0 = 4.0 kJ mol^{-1}). In (**I**–**III**)-Ar(**IV**) with E_0^{tot} = 10.1, 9.9, and 9.9 kJ mol^{-1}, Ar is also bound to the SiH_4 ligand (D_0 = 3.9, 3.9, 3.6 kJ mol^{-1}) leading to slight elongations (1–2 mÅ) of the O–H bonds involved in the DHB and small redshifts of the corresponding ν_{OH}^{b} modes by 31, 29, and 28 cm^{-1} to 2827, 2822, and 2857 cm^{-1} for **I**-Ar(**IV**), **II**-Ar(**IV**) and **III**-Ar(**IV**), respectively (Fig. S4–S6, ESI†).

As mentioned above, the IR spectra predicted for (**I**–**III**)-Ar are almost identical. Hence, for simplicity only the IR spectra calculated for **I**-Ar(**I**,**II**) and **IV**-Ar(**I**) are compared in Fig. 4 to the IRPD spectrum of $SiH_3OH_2^+SiH_4$–Ar. However, the vibrational assignments for **I**-Ar(**I**,**II**) apply equally well to **II**-Ar(**I**,**II**) and **III**-Ar(**I**,**II**). The $SiH_3OH_2^+SiH_4$–Ar spectrum also shows a significant population of isomers with a DHB, as the strong transitions **A1** and **A2** can only be assigned to $\nu_{OH}^{b(SiH_4)}$ modes of (**I**–**III**)-Ar isomers. The blueshift of band **A2** to 2910 cm^{-1} upon Ar-tagging can be explained by Ar binding to the free OH or SiH_3 groups, which leads to a contraction of the O–H bonds involved in the DHB. Therefore, **A2** is attributed to $\nu_{OH}^{b(SiH_4)}$ modes of the energetically favored (**I**–**III**)-Ar(**I**) isomers with deviations of 24, 15, and 48 cm^{-1}. However, **A2** could also be assigned to $\nu_{OH}^{b(SiH_4)}$ of (**I**–**III**)-Ar(**III**) (E_0^{tot} = 0.0, 0.3, 0.9 kJ mol^{-1}), with deviations of 9, 14, and 20 cm^{-1}. Moreover, the predicted redshifts of $\nu_{OH}^{b(Ar)}$ of (**I**–**III**)-Ar(**I**) caused by Ar-tagging also agree well with transition **C1** at 3456 cm^{-1}, with only minor deviations of 8, 14, and 14 cm^{-1}. The less blueshifted band **A1** at 2869 cm^{-1} can only be explained by $\nu_{OH}^{b(SiH_4)}$ modes of (**I**–**III**)-Ar isomers, in which Ar has a minor effect on the O–H bond involved in the DHB. To this end, band **A1** may be assigned to $\nu_{OH}^{b(SiH_4)}$ of (**I**/**II**)-Ar(**II**) (E_0^{tot} = 5.6 and 5.9 kJ mol^{-1}) at 2870/2869 cm^{-1}. However, band **A1** could also be attributed to $\nu_{OH}^{b(SiH_4)}$ of (**I**–**III**)-Ar(**IV**) (E_0^{tot} = 10.1, 10.2, 10.8 kJ mol^{-1}) although with larger deviations of 42, 47, and 12 cm^{-1}, respectively. The associated ν_{OH}^{f} modes of (**I**/**II**)-Ar(**II**) also agree well with band **E** at 3629 cm^{-1}, with deviations of 14 and 18 cm^{-1}. On the other hand, band **E** may also be assigned to ν_{OH}^{f} of (**I**–**III**)-Ar(**III**/**IV**) with deviations of less than 20 cm^{-1}. Transition **C2** at 3495 cm^{-1} cannot be explained by isomers with a DHB (**I**–**III**) and thus can only be attributed to $\nu_{OH}^{b(Ar)}$ modes of the energetically favored isomers **IV**-Ar(**I**,**II**) with Si–H–Si H-bonds (E_0^{tot} = 5.3 and 5.6 kJ mol^{-1}) with minor deviations of 13 cm^{-1}. The associated ν_{OH}^{f} modes of **IV**-Ar(**I**,**II**)

can also be attributed to band **E** with minor deviations of 4 and 5 cm^{-1}. The **IV**-Ar(**III**,**IV**) isomers can be excluded, because their $\nu_{OH}{}^{s}$ (3579/3580 cm^{-1}) and $\nu_{OH}{}^{a}$ modes (3663/3664 cm^{-1}) are not observed. In summary, the measured IRPD spectrum of $SiH_3OH_2{}^{+}SiH_4$–Ar can be fully accounted for by the three lowest-energy isomers **I**-Ar(**I**,**II**) and **IV**-Ar(**I**) representing the DHB and the CIHB, although we cannot exclude the population of similar but less stable Ar isomers. From the experimental integrated peak areas and the calculated IR intensities of the bands **A1**/**A2** and **C2**, the same population ratio as for bare $SiH_3OH_2{}^{+}SiH_4$ of 10 : 1 can roughly be estimated for (**I**–**III**)-Ar (DHB) and **IV**-Ar (CIHB), clearly favoring the DHB over the CIHB. The Ar binding energies of the isomers **I**–**IV** are in the range D_0 = 11.3–14.0 kJ mol^{-1}, while the SiH_4 binding energies are in the range D_0 = 36.2–38.9 kJ mol^{-1}, yielding a total binding energy of the order of 50 kJ mol^{-1}. This value is somewhat higher than the employed IR photon energy (<45 kJ mol^{-1}) and thus can explain that IRPD of $SiH_3OH_2{}^{+}SiH_4$–Ar causes exclusively the loss of Ar (and not Ar plus SiH_4). This consistency provides evidence that the computed interaction energies are in the correct range.

4. Further discussion

The analysis of the IRPD spectra of $SiH_3OH_2{}^{+}SiH_4$ clearly shows the preferential formation of the ionic OH···HSi DHB, while the population of isomers with a SiH···Si CIHB is substantially lower, in line with the respective computed $SiH_3OH_2{}^{+}\cdots SiH_4$ interaction energies when accounting for entropy effects. The DHBs presented here correspond to the common definition of DHBs of the type $X^{\delta-}H^{\delta+}\cdots H^{\delta-}Y^{\delta+}$, where X is more electronegative than H whereas Y is more electropositive ($EN_X > EN_H > EN_Y$). In SiH_4, the H atoms are bonded to the electropositive Si atom (Y), resulting in negatively charged H atoms that can combine with the positively charged H atoms bound to the electronegative O atom (X) of $SiH_3OH_2{}^{+}$ to form a H-bond. The DHB can be associated with two MOs (HOMO−8/9) (Fig. S8, ESI†).

In the ionic OH···HSi DHB, the calculated H···H distance (R_{HH} = 1.4 Å) is much shorter than in neutral intermolecular DHBs (*e.g.*, in amine-boranes and $ReH_5(PPh_3)_3$indole) (R_{HH} = 1.7–2.2 Å)[46,53,56] but in a similar range of other ionic DHBs such as in Ph^{+}DEMS and Ph^{+}TEMS (R_{HH} = 1.496–1.522 Å).[66] Similar to other DHBs (θ_{XHH} = 150–170°, and θ_{YHH} = 95–115°/130),[37,40,56] the O–H···H angle in the OH···HSi DHB is almost linear (θ_{OHH} = 173–176°) and the H···H–Si angle is bent (θ_{SiHH} = 125–134°). Due to the ionic character of the observed SiH···HO DHBs, the calculated binding energy (D_0 = 38.5–38.9 kJ mol^{-1}) is higher than those of neutral DHBs (16–25 kJ mol^{-1}),[33,53] but lower than of those of other ionic DHBs as, for example, observed in Ph^{+}DEMS (D_0 = 47.5–48.9 kJ mol^{-1}) or Ph^{+}TEMS (D_0 = 49.1–50.9 kJ mol^{-1}).[66] The $E^{(2)}$ energies for the interaction between the bonding σ_{SiH} orbital and the antibonding $\sigma_{OH}{}^{*}$ orbital of $SiH_3OH_2{}^{+}SiH_4$ ($E^{(2)}$ = 96–101 kJ mol^{-1}) also indicate slightly weaker DHBs compared to the DHBs of Ph^{+}DEMS and Ph^{+}TEMS ($E^{(2)}$ = 119/120 kJ mol^{-1}).[66] This view is also consistent with the experimentally observed redshifts of $\nu_{OH}{}^{b}$ modes of $SiH_3OH_2{}^{+}SiH_4$ ($\Delta\nu$ = 528/570 cm^{-1}) compared to the more redshifted $\nu_{OH}{}^{b}$ modes of Ph^{+}DEMS and Ph^{+}TEMS ($\Delta\nu$ = 674 cm^{-1}),[66] which provide a direct experimental measure of the bond strength of the H-bonds. The DHBs of $SiH_3OH_2{}^{+}$-SiH_4(**I**–**III**) appear to be slightly stronger than the CIHB in $SiH_3OH_2{}^{+}SiH_4$(**IV**) (D_0 = 39 *vs.* 36 kJ mol^{-1} at B3LYP-D3), which is detected as a minor population. The H_2O attached to the $SiH_3{}^{+}$ group significantly reduces the binding energy of the Si–H–Si H-bond preferred in silane ions, as can be seen by comparison with unperturbed $Si_2H_7{}^{+}$ (D_0 = 150 kJ mol^{-1}) or $Si_3H_{11}{}^{+}$ (D_0 = 41 kJ mol^{-1}) ions featuring one and two Si–H–Si H-bonds, respectively.[26,29] Finally, the weak Si–H–Si H-bond of $SiH_3OH_2{}^{+}SiH_4$(**IV**) is strongly asymmetric and more linear compared to the much stronger symmetric bond in $Si_2H_7{}^{+}$(R_{SiH} = 1.535/1.898 *vs.* 1.625 Å, ϕ_{SiHSi} = 160° *vs.*144°).[26,29]

5. Conclusions

The analysis of IRPD spectra of mass-selected $SiH_3OH_2{}^{+}SiH_4$ and $SiH_3OH_2{}^{+}SiH_4$–Ar clusters in the OH stretch range (2700–3800 cm^{-1}) using DFT calculations provides the first spectroscopic information about protonated silanol–silane complexes. The redshifted O–H stretch bands are clearly assigned to the energetically preferred structures (**I**–**III**) in which SiH_4 is bonded to $SiH_3OH_2{}^{+}$ *via* a dihydrogen bond (DHB) of the type $Si^{\delta+}H^{\delta-}\cdots H^{\delta+}O^{\delta-}$. Significantly, this is the first spectroscopic and structural characterization of an ionic SiH···HO DHB in a small gas-phase cluster without any interference from aromatic or aliphatic hydrocarbon structures. In addition to the structures with a DHB, a small population of the order 10% of isomer **IV** with a charge-inverted hydrogen bond (CIHB) of the type $Si^{\delta+}$–$H^{\delta-}$–$Si^{\delta+}$ is observed. Due to the OH_2 group bonded to $SiH_3{}^{+}$, the CIHB is weaker than Si–H–Si H-bonds of related $Si_xH_y{}^{+}$ cations.

Data availability

The data supporting this article have been included as part of the ESI.†

Conflicts of interest

There are no conflicts to declare.

Acknowledgements

This work was supported by Deutsche Forschungsgemeinschaft (DFG, DO 729/9). The authors thank X. N. Truong for initial support in recording the IRPD spectra.

References

1 R. D. Miller and J. Michl, *Chem. Rev.*, 1989, **89**, 1359–1410.

2 V. Chandrasekhar, R. Boomishankar and S. Nagendran, *Chem. Rev.*, 2004, **104**, 5847–5910.
3 H. Chatham and A. Gallagher, *J. Appl. Phys.*, 1985, **58**, 159–169.
4 T. P. Martin and H. Schaber, *J. Chem. Phys.*, 1985, **83**, 855–858.
5 R. Singh, *J. Phys.: Condens. Matter*, 2008, **20**, 045226.
6 V. Kumar and Y. Kawazoe, *Phys. Rev. Lett.*, 2003, **90**, 055502.
7 P. D. Lickiss, *Adv. Inorg. Chem.*, 1995, **42**, 147–262.
8 J. Fischer, J. Baumgartner and C. Marschner, *Science*, 2005, **310**, 825.
9 J. Nawrocki, *J. Chromatogr. A*, 1997, **779**, 29–71.
10 M. J. Kushner, *J. Appl. Phys.*, 1993, **74**, 6538–6553.
11 M. J. Kushner, *J. Appl. Phys.*, 1988, **63**, 2532–2551.
12 M. L. Mandich, W. D. Reents and M. F. Jarrold, *J. Chem. Phys.*, 1988, **88**, 1703–1718.
13 G. Turban, Y. Catherine and B. Grolleau, *Plasma Chem. Plasma Process.*, 1982, **2**, 61–80.
14 D. M. Goldhaber and A. L. Betz, *Astrophys. J.*, 1984, **279**, L55–L58.
15 S. Patai and Z. Rappoport, *Chem. Org. Silicon Compd.*, Wiley, Chichester, 1989.
16 K. Raghavachari, *J. Chem. Phys.*, 1988, **88**, 1688–1702.
17 K. Raghavachari, *J. Chem. Phys.*, 1990, **92**, 452–465.
18 L. A. Curtiss, H. Brand, J. B. Nicholas and L. E. Iton, *Chem. Phys. Lett.*, 1991, **184**, 215–220.
19 B. Ruscic and J. Berkowitz, *J. Chem. Phys.*, 1991, **95**, 2416–2432.
20 G. Maier, H. P. Reisenauer and J. Glatthaar, *Chem. - Eur. J.*, 2002, **8**, 4383–4391.
21 R. L. DeKock and W. B. Bosma, *J. Chem. Educ.*, 1988, **65**, 194–197.
22 J. E. McMurry and T. Lectka, *Acc. Chem. Res.*, 1992, **25**, 47–53.
23 M. Jablonski, *Chem. Phys. Lett.*, 2009, **477**, 374–376.
24 M. Jabłoński, *Struct. Chem.*, 2020, **31**, 61–80.
25 S. Civiš, M. Lamanec, V. Špirko, J. Kubišta, M. Špet'ko and P. Hobza, *J. Am. Chem. Soc.*, 2023, **145**, 8550–8559.
26 M. Savoca, J. Langer and O. Dopfer, *Angew. Chem., Int. Ed.*, 2013, **52**, 1568–1571.
27 M. A. R. George and O. Dopfer, *Int. J. Mass Spectrom.*, 2019, **435**, 51–60.
28 M. A. R. George, M. Savoca and O. Dopfer, *Chem. – Eur. J.*, 2013, **19**, 15315–15328.
29 M. A. R. George and O. Dopfer, *Phys. Chem. Chem. Phys.*, 2024, **26**, 6574–6581.
30 M. A. R. George, N. X. Truong, M. Savoca and O. Dopfer, *Angew. Chem., Int. Ed.*, 2018, **57**, 2919–2923.
31 R. Withnall and L. Andrews, *J. Phys. Chem.*, 1985, **89**, 3261–3268.
32 S. J. Grabowski, W. A. Sokalski and J. Leszczynski, *J. Phys. Chem. A*, 2004, **108**, 5823–5830.
33 S. J. Grabowski, *J. Phys. Org. Chem.*, 2013, **26**, 452–459.
34 R. H. Crabtree, *Science*, 1998, **282**, 2000–2001.
35 R. H. Crabtree, P. E. M. Siegbahn, O. Eisenstein, A. L. Rheingold and T. F. Koetzle, *Acc. Chem. Res.*, 1996, **29**, 348–354.
36 R. H. Crabtree, *Chem. Rev.*, 2016, **116**, 8750–8769.
37 R. Custelcean and J. E. Jackson, *Chem. Rev.*, 2001, **101**, 1963–1980.
38 X. Chen, J.-C. Zhao and S. G. Shore, *Acc. Chem. Res.*, 2013, **46**, 2666–2675.
39 B. G. de Oliveira, *Phys. Chem. Chem. Phys.*, 2013, **15**, 37–79.
40 T. Kar and S. Scheiner, *J. Chem. Phys.*, 2003, **119**, 1473–1482.
41 A. Filippi, A. Troiani and M. Speranza, *J. Phys. Chem. A*, 1997, **101**, 9344–9350.
42 G. N. Patwari, *J. Phys. Chem. A*, 2005, **109**, 2035–2038.
43 G.-J. Zhao and K.-L. Han, *J. Chem. Phys.*, 2007, **127**, 024306.
44 N. Mohan and C. H. Suresh, *J. Phys. Chem. A*, 2014, **118**, 1697–1705.
45 V. Sumerin, F. Schulz, M. Nieger, M. Atsumi, C. Wang, M. Leskelä, P. Pyykkö, T. Repo and B. Rieger, *J. Organomet. Chem.*, 2009, **694**, 2654–2660.
46 J. Wessel, J. C. Lee Jr, E. Peris, G. P. A. Yap, J. B. Fortin, J. S. Ricci, G. Sini, A. Albinati, T. F. Koetzle, O. Eisenstein, A. L. Rheingold and R. H. Crabtree, *Angew. Chem., Int. Ed. Engl.*, 1995, **34**, 2507–2509.
47 C. A. Morrison and M. M. Siddick, *Angew. Chem., Int. Ed.*, 2004, **43**, 4780–4782.
48 Y. Meng, Z. Zhou, C. Duan, B. Wang and Q. Zhong, *J. Mol. Struct.: THEOCHEM*, 2005, **713**, 135–144.
49 Y. Feng, S.-W. Zhao, L. Liu, J.-T. Wang, X.-S. Li and Q.-X. Guo, *J. Phys. Org. Chem.*, 2004, **17**, 1099–1106.
50 S. Marincean and J. E. Jackson, *J. Phys. Chem. A*, 2004, **108**, 5521–5526.
51 I. Rozas, I. Alkorta and J. Elguero, *J. Phys. Chem. A*, 1999, **103**, 8861–8869.
52 E. Peris, J. C. Lee Jr and J. R. Rambo, *J. Am. Chem. Soc.*, 1995, **117**, 3485–3491.
53 T. Richardson, S. de Gala, R. H. Crabtree and P. E. M. Siegbahn, *J. Am. Chem. Soc.*, 1995, **117**, 12875–12876.
54 A. J. Lough, S. Park, R. Ramachandran and R. H. Morris, *J. Am. Chem. Soc.*, 1994, **116**, 8356–8357.
55 J. C. Lee Jr, E. Peris, A. L. Rheingold and R. H. Crabtree, *J. Am. Chem. Soc.*, 1994, **116**, 11014.
56 W. T. Klooster, T. F. Koetzle, P. E. M. Siegbahn, T. B. Richardson and R. H. Crabtree, *J. Am. Chem. Soc.*, 1999, **121**, 6337–6343.
57 G. N. Patwari, T. Ebata and N. Mikami, *J. Chem. Phys.*, 2000, **113**, 9885–9888.
58 G. Naresh Patwari, T. Ebata and N. Mikami, *J. Chem. Phys.*, 2001, **114**, 8877–8879.
59 G. N. Patwari, T. Ebata and N. Mikami, *J. Phys. Chem. A*, 2001, **105**, 8642–8645.
60 G. N. Patwari, T. Ebata and N. Mikami, *Chem. Phys.*, 2002, **283**, 193–207.
61 G. Naresh Patwari, T. Ebata and N. Mikami, *J. Chem. Phys.*, 2002, **116**, 6056–6063.
62 G. N. Patwari, A. Fujii and N. Mikami, *J. Chem. Phys.*, 2006, **124**, 241103.
63 P. C. Singh and G. N. Patwari, *J. Phys. Chem. A*, 2007, **111**, 3178–3183.

64 H. Ishikawa, A. Saito, M. Sugiyama and N. Mikami, *J. Chem. Phys.*, 2005, **123**, 224309.
65 M. Uchida, T. Shimizu, R. Shibutani, Y. Matsumoto and H. Ishikawa, *J. Chem. Phys.*, 2020, **153**, 104305.
66 H. Ishikawa, T. Kawasaki and R. Inomata, *J. Phys. Chem. A*, 2015, **119**, 601–609.
67 S.-W. Hu, Y. Wang, X.-Y. Wang, T.-W. Chu and X.-Q. Liu, *J. Phys. Chem. A*, 2004, **108**, 1448–1459.
68 Y. Kawashima, R. D. Suenram and E. Hirota, *J. Chem. Phys.*, 2016, **145**, 114307.
69 O. Dopfer, *Int. Rev. Phys. Chem.*, 2003, **22**, 437–495.
70 O. Dopfer, *Z. Phys. Chem.*, 2005, **219**, 125–168.
71 M. Fujii and O. Dopfer, *Int. Rev. Phys. Chem.*, 2012, **31**, 131–173.
72 O. Dopfer and M. Fujii, *Chem. Rev.*, 2016, **116**, 5432–5463.
73 M. J. Frisch, *et al.*, *GAUSSIAN16, revision C.02*, Gaussian, Inc., Wallingford, CT, 2016.
74 N. Solcà and O. Dopfer, *Chem. Phys. Lett.*, 2000, **325**, 354–359.
75 R. V. Olkhov and O. Dopfer, *Chem. Phys. Lett.*, 1999, **314**, 215–222.
76 P. J. Linstrom and W. G. Mallard, *NIST Chemistry WebBook, NIST Standards and Technology*, Gaithersburg, MD, 2001, **https://webbook.nist.gov/**, 20899.
77 D. R. J. Boyd, *J. Chem. Phys.*, 2004, **23**, 922–926.

